CHIN. PHYS. LETT. Vol. 35, No. 8 (2018) 087303

Discovery of Two-Dimensional Quantum Spin Hall Effect in Triangular Transition-Metal Carbides *

Shou-juan Zhang(张守娟)[1], Wei-xiao Ji(纪维霄)[1], Chang-wen Zhang(张昌文)[1**], Shu-feng Zhang(张树峰)[1], Ping Li(李萍)[1], Sheng-shi Li(李胜世)[2], Shi-shen Yan(颜世申)[2**]

[1]*School of Physics and Technology, University of Jinan, Jinan 250022*
[2]*School of Physics, State Key Laboratory of Crystal Materials, Shandong University, Jinan 250100*

(Received 4 February 2018)

Though the quantum spin Hall effect (QSHE) in two-dimensional (2D) crystals has been widely explored, the experimental realization of quantum transport properties is only limited to HgTe/CdTe or InAs/GaSb quantum wells. Here we employ a tight-binding model on the basis of d_{z^2}, d_{xy}, and $d_{x^2-y^2}$ orbitals to propose QSHE in the triangular lattice, which are driven by a crossing of electronic bands at the Γ point. Remarkably, 2D oxidized Mxenes $W_2M_2C_3$ are ideal materials with nontrivial gap of 0.12 eV, facilitating room-temperature observations in experiments. We also find that the nontrivially topological properties of these materials are sensitive to the cooperative effect of the electron correlation and spin-orbit coupling. Due to the feasible exfoliation from its 3D MAX phase, our work paves a new direction towards realizing QSHE with low dissipation.

PACS: 73.43.−f, 73.43.Nq, 73.20.At DOI: 10.1088/0256-307X/35/8/087303

Topological insulators (TIs) are newly discovered quantum states in which, even though the bulk structure is insulating, the surface supports metallic electronic states with Dirac-like linear energy dispersion protected by the time-reversal symmetry (TRS) that gives rise to the nontrivial Z_2 topological invariant.[1−3] These metallic states are unique since they exhibit chirality or locking of the directions of spin and momentum, which are not allowed to scatter backward in the absence of magnetic impurities. Thus they represent the emergence of the spins in quantum materials, opening the door to exploring new fundamental science problems, including novel spin textures and superconducting states. These promising properties present an ideal material platform for designing low-dispersionless topological devices for thermoelectric, information processing, and other applications.[4,5]

As is known, band inversion (BI) in topological materials is a key factor for driving band topology. The BHZ model[6] characterized by BI induced *via* spin-orbit coupling (SOC) at time reversal invariant momenta (TRIM) between two bands of different parities, is an interesting model, which is shown in Fig. 1(a). If one tunes the SOC strength in an architected process, the topological phase transition goes through four stages: band gap decreasing (I), gap closing (II), band inversion (III), and band gap reopen (IV).[7] In this case, the band gap without SOC (stage I) seems to undermine the effectiveness of SOC in the topological phase. These are why QSHE has only been observed in HgTe/CdTe[8,9] and InAs/GaSb quantum wells,[10] though many topological materials have been theoretically predicted.[11−21] Thus the observations of QSHE in 2D crystal are still challenging experimentally.

Here by combining a tight-binding (TB) model and density-functional theory (DFT) calculations, we propose a new strategy to make SOC more effective to realize QSHE in the triangular lattice, as shown in Fig. 1(b). Here the band topology is caused by the d–d band interaction, instead of conventional s–p and p–p inversion in 2D materials. More interestingly, we find that the oxidized MXenes $W_2M_2C_3$ (M =Ti, Zr, Hf) with the triangular lattice are ideal candidate materials for realizing QSHE. These materials have a nontrivial band gap as large as 0.12 eV, facilitating room-temperature observations in experiments. Considering that such a 2D lattice is naturally stable against oxidization and degradation, our works pave a new way towards realizing QSHE in realistic materials.

We construct a low-energy Hamiltonian model for a triangular lattice, in which there is a band touch in the d-band crystals with each d element contributing three d orbitals with a minimal basis of d_{z^2}, d_{xy}, and $d_{x^2-y^2}$ orbitals, as illustrated in Figs. 1(b) and 1(c). Dominated by D_{3d} symmetry in the triangular lattice,[22] the TB Hamiltonian can be expressed as

$$\begin{aligned} H &= H_{\rm hop} + H_{\rm soc} \\ &= \begin{bmatrix} H_{\rm hop\uparrow} & 0 \\ 0 & H_{\rm hop\downarrow} \end{bmatrix} + \begin{bmatrix} H_{\rm soc\uparrow} & 0 \\ 0 & H_{\rm soc\downarrow} \end{bmatrix}, \end{aligned} \quad (1)$$

where $H_{\rm hop}$ expresses the nearest-neighboring (NN) hopping term of the sites, up and down arrows indicate respectively the spin-up and spin-down channels, and $H_{\rm soc}$ is the on-site SOC term in the Hamiltonian model.

In Eq. (1), the hoping terms can be further written

*Supported by the Natural Science Foundation of Shandong Province under Grant No ZR2018MA033, and the National Natural Science Foundation of China under Grant No 11274143.
**Corresponding author. Email: ss_zhangchw@ujn.edu.cn
© 2018 Chinese Physical Society and IOP Publishing Ltd

as

$$H = \begin{pmatrix} h_{11} & h_{12} & h_{13} \\ h_{12}^* & h_{22} & h_{23} \\ h_{13}^* & h_{23}^* & h_{33} \end{pmatrix} + \begin{pmatrix} 0 & 0 & 0 \\ 0 & 0 & -\lambda i \\ 0 & \lambda i & 0 \end{pmatrix}. \quad (2)$$

Considering that the on-site SOC term does not induce the coupling between different spin components, the spin-up and spin-down channels are separated, $H_{\mathrm{soc}\uparrow} = H_{\mathrm{soc}\downarrow}$. According to the symmetry of the triangular lattice, we can obtain the hopping terms as

$$\begin{aligned} h_{11} &= E_z + t_{zz}\Big(2\cos\Big(\frac{\sqrt{3}}{2}k_x\Big)\cos\Big(\frac{1}{2}k_y\Big) + \cos(k_y)\Big), \\ h_{12} &= -\sqrt{3}t_{zxy}\Big(2\sin\Big(\frac{\sqrt{3}}{2}k_x\Big)\sin\Big(\frac{1}{2}k_y\Big)\Big), \\ h_{13} &= t_{zxy}\Big(\cos(k_y) - cos\Big(\frac{\sqrt{3}}{2}k_x\Big)\cos\Big(\frac{1}{2}k_y\Big)\Big), \\ h_{22} &= E_{xy} + (3t\sigma + t_\pi)\cos\Big(\frac{\sqrt{3}}{2}k_x\Big)\cos\Big(\frac{1}{2}k_y\Big) \\ &\quad + 2t_\pi\cos(k_y), \\ h_{23} &= \sqrt{3}(t_\pi - t_\sigma)\sin\Big(\frac{\sqrt{3}}{2}k_x\Big)\sin\Big(\frac{1}{2}k_y\Big), \\ h_{33} &= E_{xy} + (t_\sigma + 3t\pi)\cos\Big(\frac{\sqrt{3}}{2}k_x\Big)\cos\Big(\frac{1}{2}k_y\Big) \\ &\quad + 2t_\sigma\cos(k_y), \end{aligned} \quad (3)$$

where both ε_z and ε_{xy} are the on-site energies for d_{z^2} and $d_{xy}/d_{x^2-y^2}$ orbitals, while t_{zz} and t_{zxy} are NN hopping interactions between d_{z^2} orbitals, while between d_{z^2} and $d_{xy}/d_{x^2-y^2}$ orbitals, t_σ and t_π are NN hopping interactions related to σ and π bonds formed by d_{xy} and $d_{x^2-y^2}$ orbitals, respectively.

Diagonalizing Hamiltonian H, all off-diagonal matrices at the Γ point vanish, we obtain three eigenvalues, expressed as $E^{\pm\lambda}_{d_{xy},dx^2-y^2} = 3t_\pi + 3t_\sigma + \varepsilon_{xy} \pm \lambda$, and $E_{d_{z^2}} = 3t_{zz} + \varepsilon_z$. In this case, the band structure in the basis of $d_{xy}/d_{x^2-y^2}$ and d_{z^2} orbitals per lattice site can be obtained based on the TB model Hamiltonian, as illustrated in Fig. 1(c). Note that the $d_{xy}/d_{x^2-y^2}$ bands are degenerate at the Γ point in the Brillouin zone (BZ) center, while d_{z^2} is a single state. The double degeneracy at Γ is due to the $C6$ symmetry owned by the triangular lattice. At the outset, the band structure is trivial, in which d_{z^2} is below double degenerated $d_{xy}/d_{x^2-y^2}$ bands, as shown in stage (I). This situation occurs if the on-site energy E_z is lower than that of degenerated $d_{xy}/d_{x^2-y^2}$ states. Then the topological invariant, $Z_2 = 0$, indicates a normal insulator (NI) phase. To realize a topological transition, $d_{xy}/d_{x^2-y^2}$ and d_{z^2} band inversion is needed, that is, first closing of a trivial gap followed by reopening of a nontrivial gap by changing hoping terms. Such a band inversion of $d_{xy}/d_{x^2-y^2}$ and d_{z^2} induces a parity exchange, thus the topological invariant changes from $Z_2 = 0$ to 1 (state Ⅱ). After the on-site SOC is included, the degeneracy of the $d_{xy}/d_{x^2-y^2}$ bands is lifted and band gaps are opened around these points by any finite value of 2λ, as illustrated in Fig. 1(c). Note that the d_{z^2} orbital is independent of SOC, thus the nontrivial topology is determined by the lattice, instead of SOC. As a consequence, the nontrivially topological states are realized even if the SOC is weak, as compared with the case of Fig. 1(a).

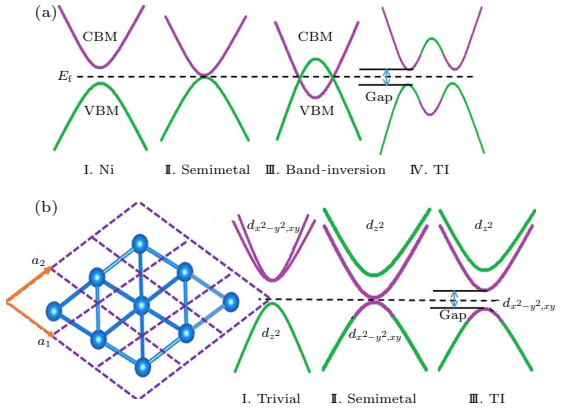

Fig. 1. Schematic plots of topological phase transition process. (a) Conventional topological phase, and (b) our proposed topological phase induced by an effective SOC.

Table 1. Lattice constant a, the buckled height h (Å), band gap E_{SOC} (eV) at Γ with SOC, and Z_2 topological invariants for $W_2M_2C_3O_2$ lattice.

Lattice	a (Å)	h (Å)	E_{SOC} (eV)	Z_2
$W_2Ti_2C_3O_2$	2.98	10.10	0.15	1
$W_2Zr_2C_3O_2$	3.09	10.52	0.19	1
$W_2Hf_2C_3O_2$	3.07	10.40	0.34	1

In the present work, we find that the oxidized $W_2M_2C_3$ (M =Ti, Zr, Hf) Mxenes are ideal candidate materials for observing QSHE, as shown in Fig. 2. This structure is composed of seven atomic layers in the sequence of W-C-M-C-M-C-W, where the transition-metal W atoms are located at the outer layers. All the calculations are performed using the VASP package[23] with generalized gradient approximation (GGA) for the correlation functional. The wave functions are constructed using a projected augmented wave approach with plane wave cutoff energy of 460 eV. The effect of SOC is included self-consistently in the electronic structure calculations. Considering that the oxygen groups are favorable to adsorb on the hollow sites of Mxene termination,[22,24,25] we focus on two types of hollow sites, which are defined as A and B in 2D $W_2M_2C_3O_2$, as depicted in Fig. 2(a). Hence, the AB model represents that O atoms on the top and bottom surfaces occupy A and B sites, respectively. Structural optimizations indicate that the AB model has the lowest energy as compared with AA and BB models. We also check its phonon dispersion spectrum using a supercell approach within the PHONON code.[26] As seen from Fig. 2(c), no appreciable imaginary phonon modes appear, indicating that 2D $W_2Ti_2C_3O_2$ is dynamic stable.

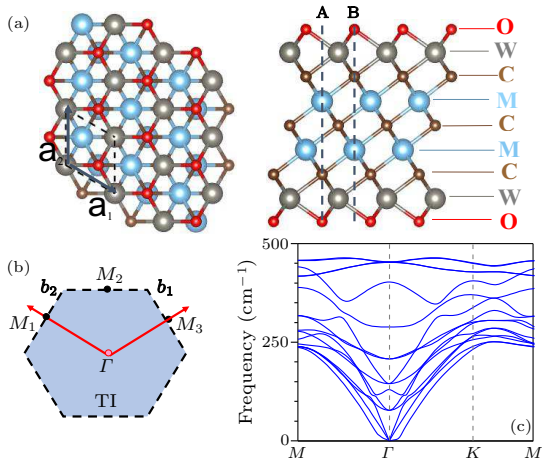

Fig. 2. (a) Top view and side view of $W_2M_2C_3O_2$ (M =Ti, Zr, or Hf) with the Bravais lattice vectors a_1 and a_2. (b) The Brillouin zones with specific symmetry points. (c) Phonon band dispersions of $W_2Ti_2C_3O_2$.

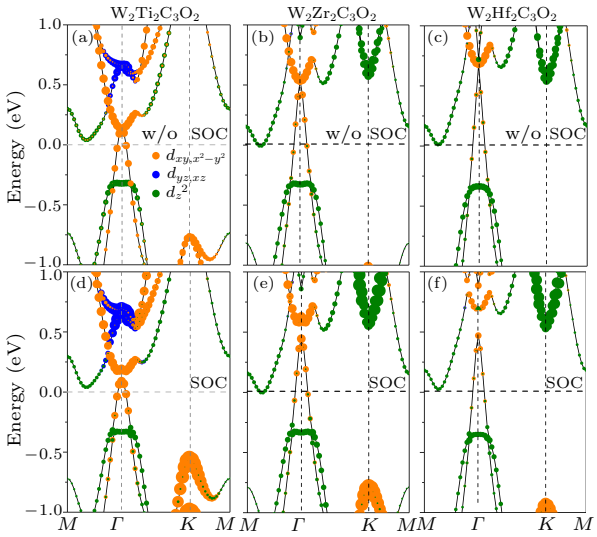

Fig. 3. Band structures calculated without SOC are shown in (a)–(c), as well as with SOC in (d)–(f). The yellow, blue, and green dots correspond to the wave function onto $d_{xy,x2-y2}$, $d_{xz,yz}$, and d_{z2} orbitals, respectively.

The electronic band structures of $W_2M_2C_3O_2$ (M =Ti, Zr, Hf) without SOC in the BZ (Fig. 2(b)) are shown in Figs. 3(a)–3(c). Note that a key feature is the band touch of the conduction band (CB) and the valence band (VB) at the Γ point. Taking $W_2Ti_2C_3O_2$ as an example, the effective masses at band edges, expressed as

$$\frac{1}{m^*} = \frac{1}{\hbar^2}\frac{\partial^2 \mathrm{E}_n(\mathrm{K})}{\partial \mathrm{K}^2}, \tag{4}$$

are $6.72m_e$ and $0.35m_e$ for electrons and holes along the Γ–K direction, respectively. Such a dramatic difference in effective mass is suitable for selectively injecting or emitting holes or electrons, enable it to promise applications in nanoelectronic devices.

Another prominent feature is that the band touch of CB and VB near the Fermi level is suspected for topological states, which motivates us to examine their nontrivial topology. Indeed, the inclusion of SOC leads to a metal-semiconductor transition, as shown in Figs. 3(d)–3(f). Its band topology can be verified by Z_2 invariant ν based on the method proposed by Fu and Kane,[27] written as

$$\delta(K_i) = \prod_{m=1}^{N} \xi_{2m}^{i}, \ (-1)^{\nu} = \prod_{i=1}^{4} \delta(K_i) = \delta(\Gamma)\delta(M)^3, \tag{5}$$

where δ is the product of parity eigenvalues at the time-reversal-invariant momenta (TRIM) points, $\xi = \pm 1$ are the parity eigenvalues, and N is the number of the occupied bands. According to the Z_2 classification, $\nu = 1$ characterizes a topologically nontrivial phase, and $\nu = 0$ is a topologically trivial phase. Because this structure is hexagonal, the parties at TRIM points including Γ (0, 0), M_1 (0, 0.5), M_2 (0.5, 0), and M_3 (0.5, 0.5) can be depicted by $-$, $+$, $+$ and $+$, respectively. Then, the Z_2 index can be simply obtained from $(-1)^{\nu} = \delta^3(M)\delta(\Gamma)$, with $Z_2 = 1$. As a consequence, the $W_2M_2C_3O_2$ lattice is topologically nontrivial.

Now, we turn to the orbital-projected band structure near the Fermi level of 2D $W_2M_2C_3O_2$. The respective weights of d bands are represented by the color code in Fig. 3. Under D_{3d} symmetry, the $3d$ states are split into three categories, including single-degenerated $A_{1g}(d_{z^2})$, double-degenerated $E_{1g}(d_{x^2-y^2,xy})$, and $E_{2g}(d_{xz,yz})$. As the interaction between low-lying C $2p$ and $3d$ orbitals is stronger, the C $2p$ orbital is pushed far away from the Fermi level, and thus is not considered here. Figure 4(c) shows the orbital level evolution of $W_2M_2C_3O_2$. In comparison to $E_{2g}(d_{xz,yz})$, $A_{1g}(d_{z^2})$ is lower due to the weak hybridization with ligand elements since it points to the center of the ligand triangle. Here $E_{2g}(d_{xz,yz})$ forms π bonds with C $2p_z$, while $E_{1g}(d_{x^2-y^2,xy})$ forms σ bonds with C (p_x, p_y) orbitals. Hence, the fact that the π interaction is weaker than the σ interaction explains why $E_{2g}(d_{xz,yz})$ has the highest energy, as shown in Fig. 3. When the chemical bonding occurs between two W atoms, $A_{1g}(d_{z^2})$ from W atoms forms bonding and antibonding states, labeled as $A_{1g}(d^{+}_{z^2})$ and $A_{1g}(d^{-}_{z^2})$, where the subscripts $+$, $-$ denote the even and odd parities, respectively. Obviously, one can see that the external strains lead to a transition from a trivial phase to a nontrivial topological phase (Ⅱ). On this occasion, a band inversion occurs between $E_{1g}(d^{+}_{x^2-y^2,xy})$ with parity $p = 1$ and A_{1g} $(d^{-}_{z^2})$ with parity $p = -1$, which leads to the nontrivial topology, as shown in stage (Ⅲ). When switching SOC on, $E_{1g}(d^{+}_{x^2-y^2,xy})$ is lifted out with unchanged parities (stage Ⅳ), and thus band inversion at the Γ point is the intrinsic characteristic of $W_2M_2C_3O_2$. Here the role of SOC is only to break the degeneracy of $E_{1g}(d^{+}_{x^2-y^2,xy})$ at the touching point, but does not serve to exchange the parity eigenvalue, which is consistent with our proposed TB model.

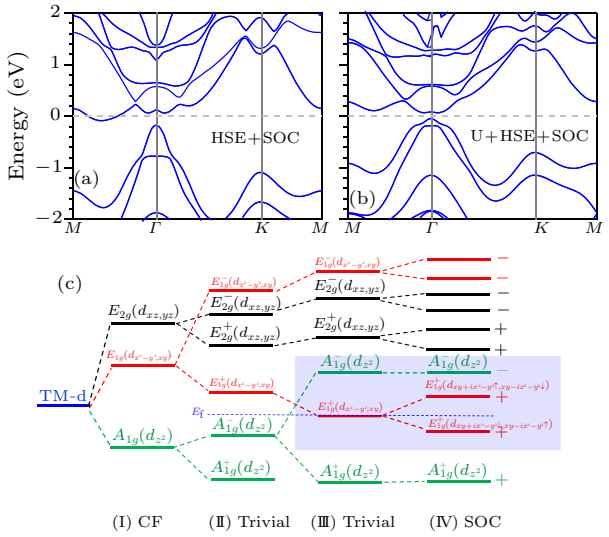

Fig. 4. Calculated results using (a) HSE06 and (b) GGA+U. The parities of the Bloch states near the Fermi level at the time-reversal invariant moment at Γ are denoted by + and −. (c) Schematic representation of the band inversion for $W_2M_2C_3O_2$ at the Γ point.

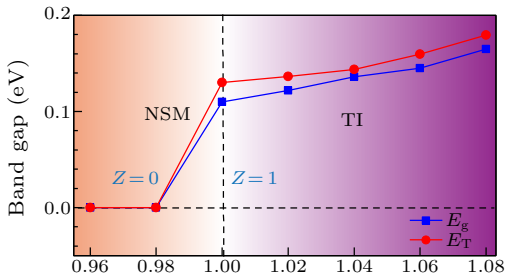

Fig. 5. Evolution of band structures, including direct-gap (E_Γ) at the Γ point and whole-gap (E_g), as a function of strain for $W_2Ti_2C_3O_2$.

To show the robust band topology of $W_2M_2C_3O_2$, we further explore the electronic structure under strain ε, which is defined as $\varepsilon = (a - a_0)/a_0$, where $a(a_0)$ is the strained (equilibrium) lattice constant. Figure 5 shows the evolution of direct gap (E_Γ) at the Γ point and the whole indirect gap (E_g) as a function of strain. Note that the band gap is sensitive to lattice change: the larger the strain is applied, the longer the M–X bond length, and the weaker the orbital hybridization between d orbitals, finally leading to the CBM levels shifting up. More interestingly, with the increase of strain, the band gap of $W_2Ti_2C_3O_2$ becomes larger. On this occasion, the band components near the Fermi energy changes qualitatively at the Γ point, where the topmost VB is composed of $A_{1g}(d^-_{z^2})$, while the lowest CBs are double-degenerate $E_{1g}(d^+_{x^2-y^2,xy})$. The band inversion indicates a topological transition from a nontrivial state to a trivial state.

Generally, the GGA underestimates the band gap of 2D materials,[28–32] an improvement is to adopt HSE06, which employs a screened exchange interaction while keeping the long-ranged Coulomb interaction. Indeed, the band gap can be enhanced to 0.12 eV, as shown in Fig. 4(a), which is far beyond room-temperature in experiments. Here we must point out that, although the bulk gap is enhanced with HSE06, the band inversion between degenerate $E_{1g}(d^+_{x^2-y^2,xy})$ and $A_{1g}(d^-_{z^2})$ is preserved, indicating that the nontrivial topology is robust. Such a large nontrivial band gap of $W_2M_2C_3O_2$ without chemical adsorption is beneficial to future experimental preparation, and makes it highly adaptable to various application environments.

Additionally, the correlation effect in d electrons of transition metals is of importance for band structures. We thus perform the GGA+U calculations with $U = 3.0$ eV for $W_2Ti_2C_3O_2$. Note that the band gap depends on the Hubbard U value: stronger electron correlation leads to a larger band gap, as shown in Fig. 4(b). Due to the poor screening of the Coulomb interaction in 2D films, it is expected that the Hubbard U in $W_2Ti_2C_3O_2$ would be larger, thus its real band gap should be enhanced significantly. When SOC is switched off, the system still keeps semi-metal even considering the effect of U. Hence, the band gap opening is a result of the cooperative effect of electron correlation and SOC, in analogy to that in Sr_2IrO4,[33] $LaCoO_3$,[34] and Nb_2O_3 crystals.[35]

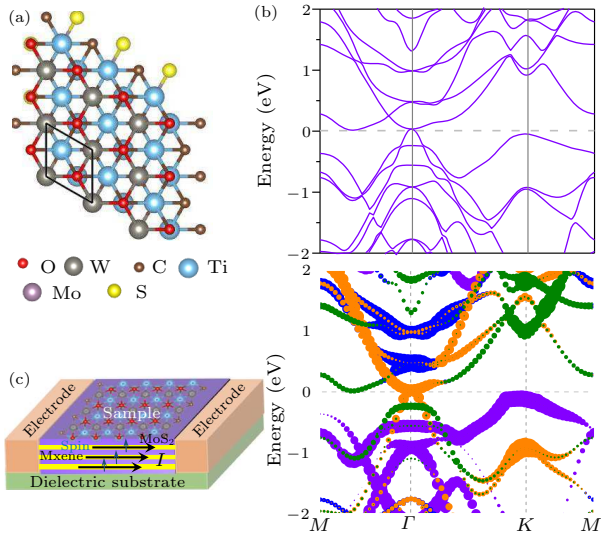

Fig. 6. (a) Top view of epitaxial growth $W_2Ti_2C_3O_2$ on MoS_2, and (b) band structure. (c) Schematic model for the quantum state measurement. Vertical arrows show the spin orientation of electrons in edge states, and horizontal arrows show their transport directions.

The distinct feature of $W_2M_2C_3$ is that it is intrinsic TIs with the Fermi level lying in the nontrivial SOC gap. Thus the synthesis of $W_2M_2C_3$ (M =Ti, Zr, Hf) is an interesting work. Currently, 2D Mxene has exfoliated from 3D phases.[36–38] To realize their potential applications, one can construct heterostructure (HTS) with MoS_2 substrates, as shown in Fig. 6(a). Since the electronic states of MoS_2 are far away from the Fermi level, the metallic edge states are immune to the presence of nonmagnetic impurities because of the protection of TRS, as shown in Fig. 6(b). The

QSHE can be realized in HTS as schematically shown in Fig. 6(c). We believe that our present work may provide an ideal platform and stimulate new experimental investigations on 2D layered structures.

In summary, we have proposed a new notion of topological phase transition from a trivial phase to a nontrivial phase with SOC and D_{3d} symmetry in Mxene structures, and present a valuable TB model. Interestingly, $W_2Ti_2C_3O_2$ has a nontrivial band gap reaching up to 0.12 eV. The sensitivity of nontrivial topology on the cooperative effect of the electron correlation and SOC is explored. Our findings present an ideal platform to search for large-gap d band TIs in 2D materials.

References

[1] Qi X L and Zhang S C 2011 *Rev. Mod. Phys.* **83** 1057
[2] Yan B H and Zhang S C 2012 *Rep. Prog. Phys.* **75** 096501
[3] Bernevig B A and Zhang S C 2006 *Phys. Rev. Lett.* **96** 106802
[4] Bansil A, Lin H and Das T 2016 *Rev. Mod. Phys.* **88** 021004
[5] Liu C C, Feng W X and Yao Y G 2011 *Phys. Rev. Lett.* **107** 076802
[6] Monkhorst H J and Pack J D 1976 *Phys. Rev.* B **13** 5188
[7] Murakami S 2007 *New J. Phys.* **9** 356
[8] König M, Wiedmann S, Brüne C, Roth A, Buhmann H, Molenkamp L W, Qi X L and Zhang S C 2007 *Science* **318** 766
[9] Zimmermann H, Keller R C, Meisen P and Seelmann-Eggebert M 1997 *Surf. Sci.* **377-379** 904
[10] Knez I, Du R R and Sullivan G 2011 *Phys. Rev. Lett.* **107** 136603
[11] Liu C X, Hughes T L, Qi X L, Wang K and Zhang S C 2008 *Phys. Rev. Lett.* **100** 236601
[12] Wang Y P, Ji W X, Zhang C W, Li P, Wang P J, Kong B, Li S S, Yan S S and Liang K 2017 *Appl. Phys. Lett.* **110** 233107
[13] Ma Y D, Dai Y, Kou L Z, Frauenheim T and Heine T 2015 *Nano Lett.* **15** 1083
[14] Wang Y P, Ji W X, Zhang C W, Li P, Zhang S F, Wang P J, Li S S and Yan S S 2017 *Appl. Phys. Lett.* **110** 213101
[15] Wang Y P, Ji W X, Zhang C W, Li P, Li F, Wang P J, Li S S and Yan S S 2016 *Appl. Phys. Lett.* **108** 073104
[16] Xu Y, Tang P Z and Zhang S C 2015 *Phys. Rev.* B **92** 081112
[17] Lima E N and Schmidt T M 2015 *Phys. Rev.* B **91** 075432
[18] Nourbakhsh Z and Vaez A 2016 *Chin. Phys.* B **25** 037101
[19] Zhang R W, Zhang C W, Ji W X, Li S S, Hu S J, Yan S S, Li P, Wang P J and Li F 2015 *New J. Phys.* **17** 083036
[20] Li S S, Ji W X, Hu S J, Zhang C W and Yan S S 2017 *EACS Appl. Mater. Inter.* **9** 41443
[21] Zhao H, Zhang C W, Ji W X, Zhang R W, Li S S, Yan S S, Zhang B M, Li P and Wang P J 2016 *Sci. Rep.* **6** 20152
[22] Weng H M, Ranjbar A, Liang Y Y, Song Z D, Khazaei M, Yunoki S, Arai M, Kawazoe Y, Fang Z and Dai X 2015 *Phys. Rev.* B **92** 075436
[23] Kresse G and Furthmüller J 1996 *Phys. Rev.* B **54** 11169
[24] Khazaei M, Arai M, Sasaki T, Estili M and Sakka Y 2014 *Phys. Chem. Chem. Phys.* **16** 7841
[25] Wang F, Yang C, Duan C, Xiao D, Tang Y and Zhu J 2014 *J. Electrochem. Soc.* **162** B16
[26] Parlinski K, Li Z Q and Kawazoe Y 1997 *Phys. Rev. Lett.* **78** 4063
[27] Fu L and Kane C L 2007 *Phys. Rev.* B **76** 045302
[28] Weng H M, Dai X and Fang Z 2014 *Phys. Rev.* X **4** 011002
[29] Sun Y, Felser C and Yan B H 2015 *Phys. Rev.* B **92** 165421
[30] Zhou L J, Kou L Z, Sun Y, Felser C, Hu F M, Shan G C, Smith S C, Yan B H and Frauenheim T 2015 *Nano Lett.* **15** 7867
[31] Perdew J P and Wang Y 1992 *Phys. Rev.* B **45** 13244
[32] Grimme S 2006 *J. Comput. Chem.* **27** 1787
[33] Kim B J, Jin H, Moon S J, Kim J Y, Park B G, Leem C S et al 2008 *Phys. Rev. Lett.* **101** 076402
[34] Wang Y L, Wang Z J, Fang Z and Dai X 2015 *Phys. Rev.* B **91** 125139
[35] Zhang S J, Zhang C W, Zhang S F, Ji W X, Li P, Wang P J, Li S S and Yan S S 2017 *Phys. Rev.* B **96** 205433
[36] Naguib M, Kurtoglu M, Presser V, Lu J, Niu J J, Heon M, Hultman L, Gogotsi Y and Barsoum M W 2011 *Adv. Mater.* **23** 4248
[37] Naguib M, Mashtalir O, Carle J, Presser V, Lu J, Hultman L, Gogotsi Y and Barsoum M W 2012 *ACS Nano* **6** 1322
[38] Yang J, Naguib M, Ghidiu M, Pan L M, Gu J, Nanda J, Halim J, Gogotsi Y, Barsoum M W and Zhou Y 2016 *J. Am. Ceram. Soc.* **99** 660